

*Carnegie Observatories Astrophysics Series, Vol. 3:  
Clusters of Galaxies: Probes of Cosmological Structure and Galaxy Evolution  
ed. J. S. Mulchaey, A. Dressler, and A. Oemler (Cambridge: Cambridge Univ. Press)*

# Clustering Studies with the 2dF Galaxy Redshift Survey

WARRICK J. COUCH<sup>1</sup>, MATTHEW M. COLLESS<sup>2</sup>, and ROBERTO DE PROPRIS<sup>2</sup>

(1) School of Physics, University of New South Wales, Sydney, Australia

(2) Research School of Astronomy & Astrophysics, Australian National University, ACT, Australia

## Abstract

The 2dF Galaxy Redshift Survey has now been completed and has mapped the three-dimensional distribution, and hence clustering, of galaxies in exquisite detail over an unprecedentedly large ( $\sim 10^8 h^{-3} \text{ Mpc}^3$ ) volume of the local Universe. Here we highlight some of the major results to come from studies of clustering within the survey: galaxy correlation function and power spectrum analyses and the constraints they have placed on cosmological parameters; the luminosity functions of rich galaxy clusters, their dependence on global cluster properties and galaxy type, and how they compare with the field; and the variation of galactic star formation activity with environment, both within clusters and in galaxy groups.

## 1.1 Introduction

Given the long and distinguished record the Carnegie Observatories have in the exploration of galaxies and determining their distances from us, it is perhaps fitting that this centennial celebration coincides with the emergence of the new generation of large galaxy redshift surveys that are now mapping the galaxy distribution over statistically representative ( $\sim 10^8 h^{-3} \text{ Mpc}^3$ ) volumes of the local Universe. The 2dF Galaxy Redshift Survey (2dFGRS; Colless et al. 2001), carried out on the 3.9 m Anglo-Australia Telescope at Siding Spring Observatory, Australia, is one such survey. Unlike the Sloan Digital Sky Survey (Nichol 2003), the 2dFGRS has already been completed, with its final observations taken on 11 April 2002. At that point it had obtained spectra for 270,000 objects, providing redshifts for 221,496 unique galaxies in the range  $0.0 \leq z \leq 0.3$ , with a median of  $z = 0.11$ .

The survey provides an almost complete sampling of the galaxy distribution down to an extinction-corrected limit of  $b_J = 19.45$  mag over  $\sim 1800$  square degrees of sky. This sky coverage is contained within two declination strips covering  $75^\circ \times 10^\circ$  and  $80^\circ \times 15^\circ$  in the NGP and SGP regions, respectively, plus 99 “random” 2-degree fields in the SGP. The contiguous coverage of the sky within the two strips, together with the almost complete ( $\sim 95\%$ ) sampling of the galaxy distribution, has produced the highest fidelity three-dimensional (3D) maps ever seen of the galaxy distribution and its large-scale structure. This is clearly revealed in the cone diagram shown in Figure 1.1, where the full range of structures (knots, filaments, voids) are resolved in fine and delicate detail.

One of the most conspicuous features of the galaxy distribution seen in Figure 1.1 is the *clustering* of galaxies, and the abundance of dense, “knotty” structures in which rich

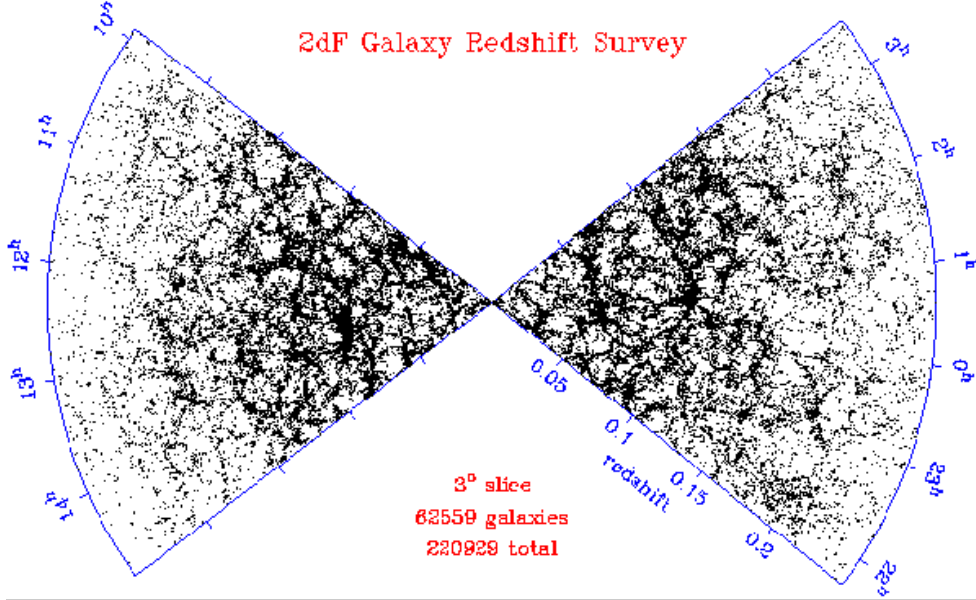


Fig. 1.1. A cone diagram based on a 3-degree slice taken through the NGP (left) and SGP (right) strips of the 2dFGRS.

clusters are embedded. It is the quantification of this clustering and the rich wealth of data on clusters (and their environs) that the 2dFGRS has provided that is the focus of this paper. Firstly, we briefly review the key findings to come from the precision measurements of galaxy clustering afforded by 2dFGRS, many of which have become the “flagship” results of the survey. We then describe the work that we have been doing on *known* rich clusters within the survey, using them as sites to study the galaxy luminosity function (LF) and galactic star formation in the densest environments, and hence via contrast with these same properties measured in lower-density regions within the survey, to draw conclusions as to their environmental dependence. Finally, we briefly mention work in progress on using the survey itself to generate a new 3D-selected catalog of galaxy groups and clusters using automated and objective group-finding algorithms.

## 1.2 Galaxy Clustering: Key Results

In quantifying and characterizing the clustering seen in the 3D galaxy distribution, 2dFGRS has realized significant advances, not just in the precision of the measurements, but also in extending them to much larger scales. The key to the latter is the much larger volumes that are (sparsely) probed by the random fields (cf. the strips on their own), allowing structure to be measured on scales up to  $400h^{-1}$  Mpc.

The clustering over these scales has been measured statistically using both two-point correlation function and power spectrum analyses. Being based on redshift information, these functions are, of course, derived in terms of the redshift-space rather than the real-space positions of galaxies. Nonetheless, when used jointly and in combination with the matter power spectrum provided by cosmic microwave background measurements, they have yielded a

number of new fundamental results on the origin of large-scale structure, the matter content and density of the Universe, and galaxy biasing; these can be summarized as follows (for further details, see the specific references quoted and also Colless 2003):

- (1) Unambiguous detection of coherent collapse on large scales — manifested by a flattening of the 2D correlation function in the line-of-sight direction at scales of  $20\text{--}40 h^{-1} \text{ Mpc}$  — confirming structures grow via gravitational instability (Peacock et al. 2001).
- (2) The detection in the power spectrum of “acoustic” oscillations due to baryon-photon coupling in the early Universe. Derivation from these oscillations of the baryon fraction:  $\Omega_b/\Omega_m = 0.17 \pm 0.06$  (Percival et al. 2001).
- (3) Measurement of  $\Omega_m$  from both the power spectrum and the redshift-space distortions seen in the 2D correlation function:  $\Omega_m = 0.30 \pm 0.06$ .
- (4) Through comparison of the 2dFGRS power spectrum and the cosmic microwave background power spectrum, the first measurement of the galaxy bias parameter  $b^* = 0.96 \pm 0.08$  (Lahav et al. 2002; see also Verde et al. 2002) and its variation with galaxy luminosity ( $b/b^* = 0.85 + 0.15L/L^*$ ; Norberg et al. 2001) and type (Madgwick et al. 2003).
- (5) Placement of a stronger limit on the neutrino fraction,  $\Omega_\nu/\Omega_m < 0.13$ , implying a limit on the mass of all neutrino species of  $m_\nu < 1.8 \text{ eV}$  (Elgarøy et al. 2002).

### 1.3 Cluster Luminosity Functions

The 2dFGRS includes an abundance of rich clusters, with 947 known clusters from the Abell (Abell 1958; Abell, Corwin, & Olowin 1989), APM (Dalton et al. 1997) and EDCC (Lumsden et al. 1992) catalogs identified and further characterized by De Propris et al. (2002) at a time when the survey was just half complete. Of these, 60 have since been used for a detailed study of the cluster LF (De Propris et al. 2003). Here the selection was restricted to clusters with  $z < 0.11$  in order to sample well below the predicted  $M^*$ . A further criterion was that clusters must contain at least 40 confirmed members within the Abell radius ( $1.5 h^{-1} \text{ Mpc}$ ). Cluster membership had been determined previously in the De Propris et al. (2002) study using a “gapping” algorithm to isolate cluster galaxies in redshift space. The clusters were also chosen to ensure a range in velocity dispersion (and hence mass), richness, Bautz-Morgan (B-M) type, and structural morphology.

This sample was used to produce a series of “composite” LFs, with clusters and their member galaxies being combined to allow meaningful and statistically robust comparisons based on both global cluster properties and galaxy type. As a starting point, a composite LF was derived for the entire cluster sample containing 4186 members; this is shown in Figure 1.2. As can be seen, it provides a very high-quality “overall” cluster LF covering 7.5 magnitudes in luminosity ( $-22 < M_{b_J} < -16$ ). It is well fit by a Schechter (1976) function with a characteristic magnitude of  $M_{b_J}^* = -20.07 \pm 0.07$  and a faint-end slope of  $\alpha = -1.28 \pm 0.03$  (right-hand panel of Fig. 1.2).

A series of composite LFs based on global cluster properties were also constructed, with the cluster sample divided into subsamples according to high ( $\sigma_v \geq 800 \text{ km s}^{-1}$ )/low ( $\sigma_v < 800 \text{ km s}^{-1}$ ) velocity dispersion, rich/poor, “early” B-M (Types I, I-II, II)/“late” B-M (Types II-III, III), and with substructure/without substructure (see De Propris et al. 2003 for further details). Surprisingly, no statistically significant LF variation was seen between these different subsamples! The only conspicuous difference seen was between composite LFs formed for the inner (core) and outer regions of clusters, with the former having many more very bright galaxies than the latter.

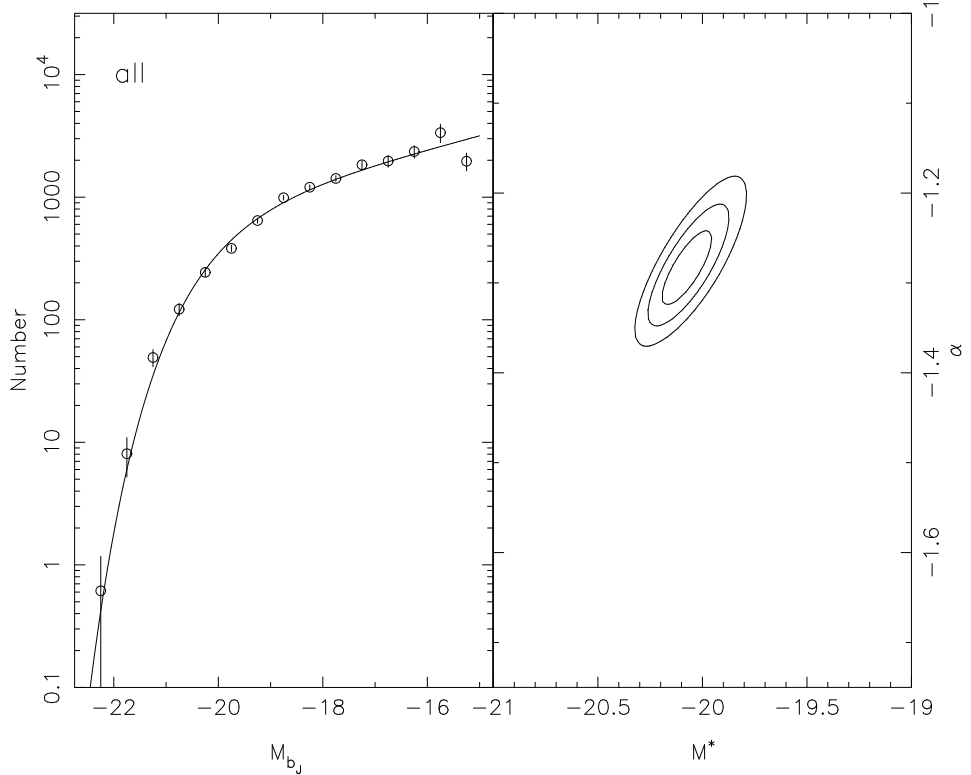


Fig. 1.2. *Left panel:* The composite LF measured for 60 known rich clusters in the 2dFGRS. *Right panel:* Error contours for the  $M^*$  and  $\alpha$  parameter values from a Schechter function fit to this composite LF.

Comparison of these composite cluster LFs, in particular the “overall” function shown in Figure 1.2, with their 2dFGRS field counterparts is readily available from the work of Madgwick et al. (2002). A Schechter function fit to their composite field LF over the same absolute magnitude range yields parameter values of  $M_{bJ}^* = -19.79 \pm 0.07$  mag and  $\alpha = -1.19 \pm 0.03$ . Hence, taken at face value, it would appear that the cluster LF is 0.3 mag brighter in  $M_{bJ}^*$  and has a steeper faint-end slope ( $\alpha_{clus} - \alpha_{fld} = -0.1$ ).

However, clusters contain a very different morphological mix of galaxies compared to the low-density field (Oemler 1974; Dressler 1980), and before this difference in the LFs between the two can be interpreted as evidence for an environmental dependence, underlying LF-galaxy type effects (which have already been seen in the field; Folkes et al. 1999; Madgwick et al. 2002) need to be first investigated. This has been done on the basis of galaxy spectral type, paralleling the approach taken by Madgwick et al. (2002) for the field. Here, a galaxy’s spectrum is typed on the basis of the relative strength of its first two principal components (from a principal component analysis analysis; Folkes et al. 1999), which represent the emission and absorption components within the spectrum. This is parameterized in terms

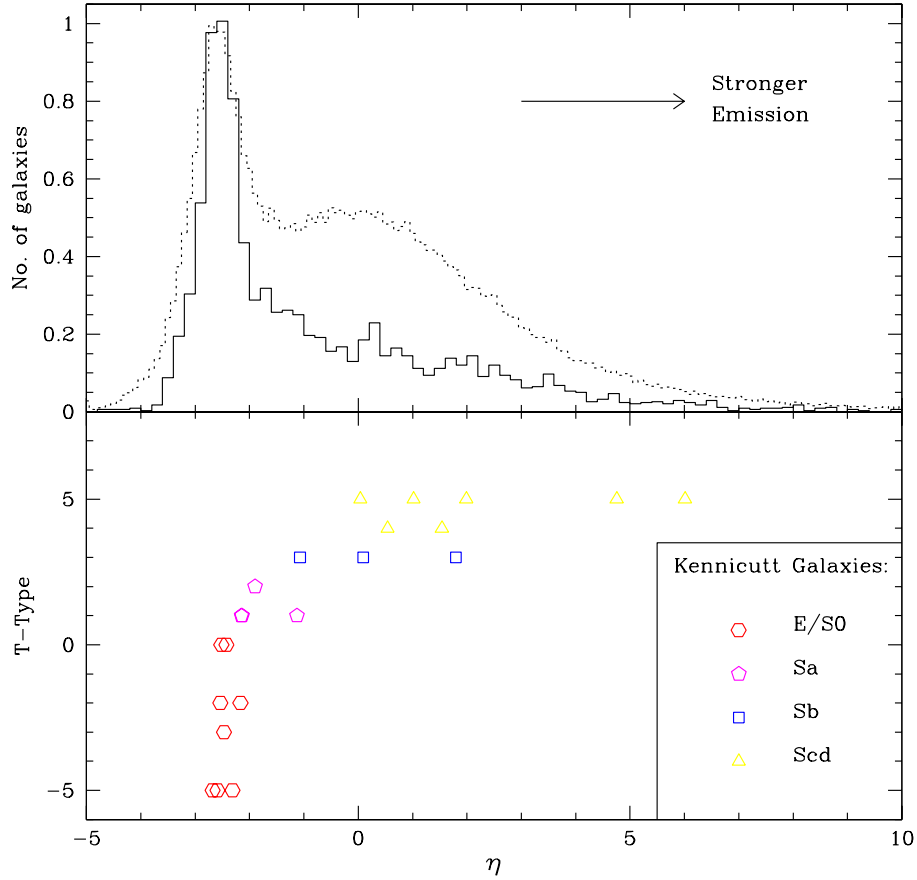


Fig. 1.3. *Upper panel:* Distribution of different spectral types (as measured by the  $\eta$  parameter; see text for details) within our clusters (solid line) and in the general field (dotted line). *Lower panel:* Relationship between galaxy morphology, represented by T type, and  $\eta$ .

of the quantity  $\eta$ , which is the linear combination of these two components:  $\eta = a pc_1 - pc_2$ . As might be expected, clusters and the field have quite a different mix of galaxies in terms of  $\eta$ , as can be seen in the upper panel of Figure 1.3. In line with the morphology-density relation (Dressler 1980) and the relationship between  $\eta$  and morphology (T type) that is seen in the bottom panel of Figure 1.3, clusters are dominated by galaxies with the lowest  $\eta$  values (absorption-line dominated, no emission), whereas the field contains a much larger proportion of galaxies with higher ( $\eta > 0$ ) values, indicative of line emission in what are most likely late-type spirals. For the purposes of deriving LFs for different spectral types, Madgwick et al. (2002) divided the  $\eta$  scale into 4 intervals, with Type 1 galaxies being those in the range  $-5 < \eta \leq -1.3$ , Type 2 galaxies  $-1.3 < \eta \leq 1.1$ , Type 3 galaxies  $1.1 < \eta \leq 3.4$ , and Type 4 galaxies  $\eta > 3.4$ .

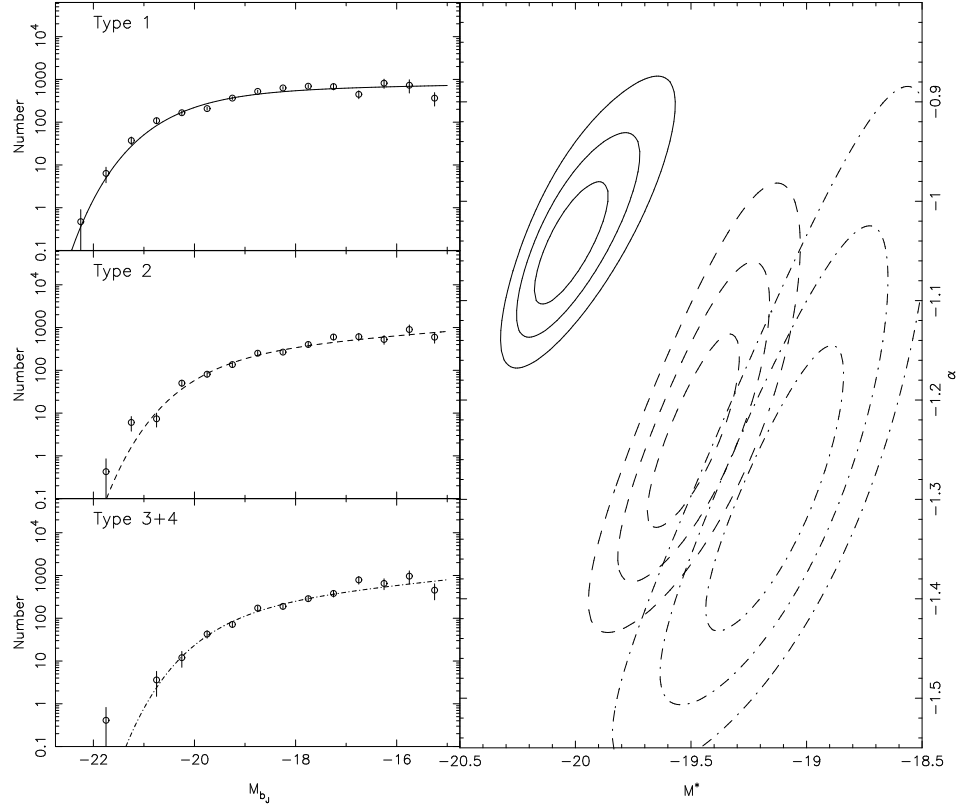


Fig. 1.4. *Left panel:* LFs for galaxies of different spectral types within clusters. *Right panel:* The 1, 2, and 3  $\sigma$  error contours for the  $M_{b_J}^*$  and  $\alpha$  values from the Schechter function fits to these LFs.

Using these same definitions, De Propris et al. (2003) derived composite LFs for the Type 1, Type 2, and Types 3+4 galaxies within their clusters; these are plotted in the left-hand panel of Figure 1.4. Here we see the same general trends that are seen in the field (Madgwick et al. 2002) in that earlier spectral types have LFs with brighter characteristic magnitudes and flatter faint-end slopes. This can be seen quantitatively in the right-hand panel of Figure 1.4. However, careful comparison of these LFs with their field counterparts (Fig. 1.5) reveals some subtle, but significant, differences, at a level of detail only a large survey like 2dFGRS can discern.

These differences are encapsulated in Figure 1.6, which shows the location in the  $\alpha - M_{b_J}^*$  plane of the Type 1, Type 2, and Type 3+4 LFs both for clusters and the field, as well as the “overall” LFs based on all types. Clearly the biggest difference between cluster and field is for the early types, with the cluster Type 1 LF having a brighter  $M_{b_J}^*$  (by  $\sim 0.5$  mag) and a steeper faint-end slope ( $\alpha_{cl} - \alpha_{fld} = -0.5$ ) compared to the field. In contrast, the cluster and field LFs for the latest types (Types 3 and 4) are, to within the errors, indistinguishable.

The type-dependent differences in the Schechter LF parameters that are seen between

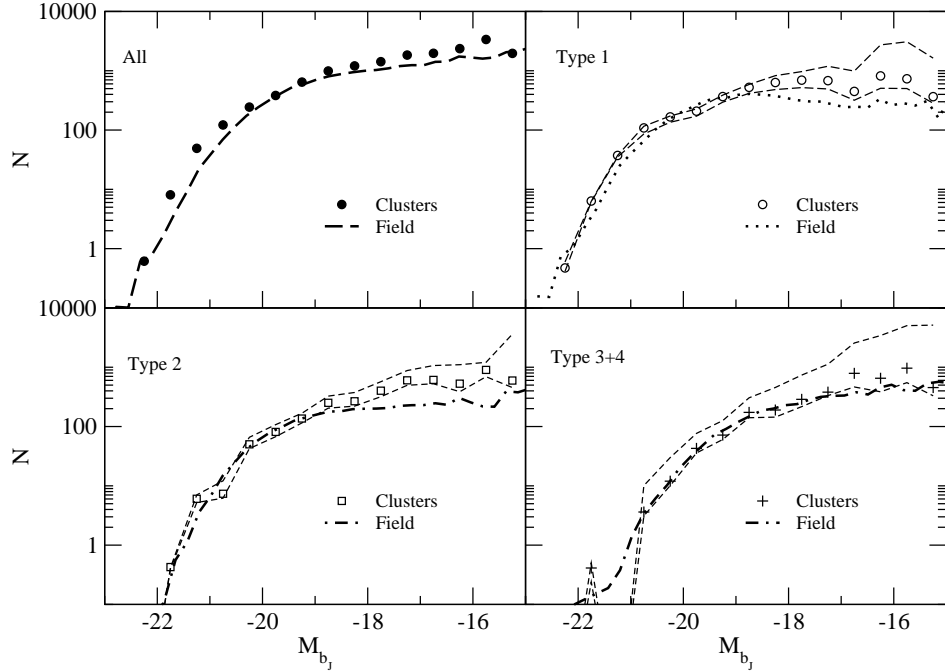


Fig. 1.5. Comparison of cluster and field LFs. The *points* represent the cluster data shown in the previous two figures. The *thick dashed lines* in each panel represent the 2dFGRS field data from Madgwick et al. (2002). The *thin dashed lines* provide representations of the cluster data with no completeness correction (*lower*) and maximum completeness correction (*upper*); see De Propris et al. (2003) for further details.

clusters and the field in Figure 1.6 also put the comparison of the “overall” LFs into perspective. Although there is a significant difference between the two, it is small in comparison to the differences seen between the early types (Types 1 and 2). This, together with the quite different mix of spectral types in clusters and in the field, would indicate that the similarity in the overall LFs is more by accident than design, with these mix and spectral type effects conspiring to produce LFs in the two different environments with characteristic magnitudes and faint-end slopes that are quite similar.

In order to understand these type-dependent LF differences between clusters and the field in the context of cluster galaxy and environment-dependent evolution, an initial attempt has been made to model them using a simple “closed box” approach (De Propris et al. 2003). This involves making the following basic assumptions: (1) cluster galaxies have evolved from field galaxies contained within the volume that collapses to become the cluster, (2) this evolution is characterized by a suppression of star formation activity and an accompanying change in spectral type, and (3) the number of galaxies is conserved (i.e., mergers are neglected). Under these assumptions, the type-specific field LFs are taken to be the initial LFs

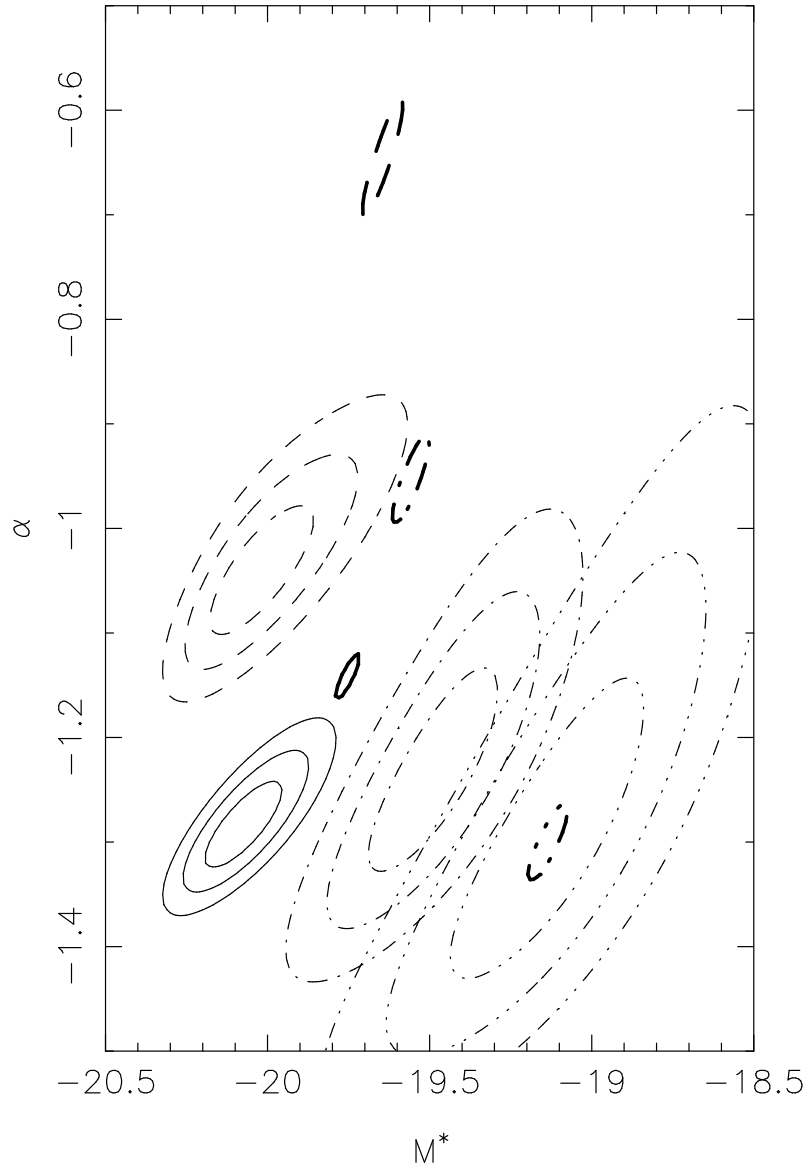


Fig. 1.6. Error ellipses for the Schechter function fits to the cluster (thin lines) and field (thick lines) LFs. *Dashed lines*: Type 1 galaxies; *dot-dashed lines*: Type 2 galaxies; *dotted-dashed lines*: Types 3+4. Only the  $3\sigma$  error ellipse is shown for the field data.

within the cluster volume, with the relative normalizations set by the mix of different types that are observed.

This very simple model has some success in that it reproduces the similar shape but

*W. J. Couch, M. M. Colless, and R. De Propris*

different normalization that is observed for the Type 3+4 LFs in clusters and in the field. Moreover, it does cause the initial field LFs of the Type 1 and 2 galaxies to evolve toward the forms they are observed to have in clusters. However, at a more detailed level, it fails in producing too many bright Type 2 cluster galaxies, too few very bright Type 1 cluster galaxies, and too few faint Type 1 cluster galaxies. Obvious refinements to this model (on which we are currently working) are to allow for luminosity-dependent fading to steepen the faint-end slopes of the earlier types, and to include mergers to explain the excess of very bright early types at the expense of their fainter counterparts.

## 1.4 Star Formation Versus Environment

The galaxy spectra obtained by the 2dFGRS are of sufficient quality not only to determine redshifts but also to measure spectral-line indices and derive astrophysical information about the galaxies themselves. Moreover, the spectra extend to sufficiently red wavelengths ( $\lambda \approx 8500 \text{ \AA}$ ) to include the redshifted  $\text{H}\alpha$  emission (or absorption) line, thus providing a reliable means of measuring the overall star formation rate (SFR) within galaxies (Kennicutt 1992). In this section we describe how this has been used to track star formation activity as a function of environment, firstly from a cluster-centric point of view, and secondly in galaxy groups.

### 1.4.1 Within Rich Clusters

To date, the global SFR among galaxy populations has generally concentrated on the two extremes of galaxy environment: the low-density field and the dense cores of rich clusters. For the latter, attention has been very much drawn by the discovery of Butcher & Oemler (1978) that such systems harbored many more star-forming galaxies in the past. But galaxies in cluster cores comprise only a small fraction of the stellar content of the Universe and may be subject to environmental effects that are peculiar to these very high-density environments (e.g., ram pressure stripping, galaxy “harassment,” and tidal interactions; Dressler 2003). Much more pertinent to the evolution of the general galaxy population is the environment *between* cluster cores and the field, spanning 3 orders of magnitude in galaxy density and which remains largely uncharted in terms of tracking star formation.

As a first step toward redressing this situation, we have analyzed 17  $z \approx 0.05 - 0.1$  clusters from the De Propris et al. (2002) study, using them to trace the global galactic SFR continuously from their centers out to arbitrarily large radii. These clusters were chosen so that roughly half (10) had “high” velocity dispersions ( $\sigma_v > 800 \text{ km s}^{-1}$ ) and the other half had “low” velocity dispersions ( $400 \leq \sigma_v \leq 800 \text{ km s}^{-1}$ ). All the 2dFGRS galaxies within a projected distance of 20 Mpc from the centers of these clusters and within the range  $0.06 < z < 0.10$  were selected for analysis. The restriction in redshift was to limit the effects of aperture bias and poor sky subtraction. A luminosity cutoff of  $M_{b_J} = -19$  mag was then applied to the sample, this being the limit to which 2dFGRS is complete over the adopted redshift range. Finally, all galaxies for which there were continuum/line fitting problems at  $\text{H}\alpha$  or whose  $\text{EW}([\text{N II}] \lambda 6583)/\text{EW}(\text{H}\alpha)$  ratios showed evidence of a nonstellar component (values  $> 0.55$ ) were excluded from the analysis. This resulted in a final sample of 11,006 galaxies.

The equivalent width of the  $\text{H}\alpha$  line (be it in absorption or emission) was measured using an automated Gaussian profile fitting algorithm, which simultaneously fitted and deblended the  $\text{H}\alpha$  line from the neighboring  $[\text{N II}] \lambda 6548 \text{ \AA}$  and  $[\text{N II}] \lambda 6583 \text{ \AA}$  lines. Since only

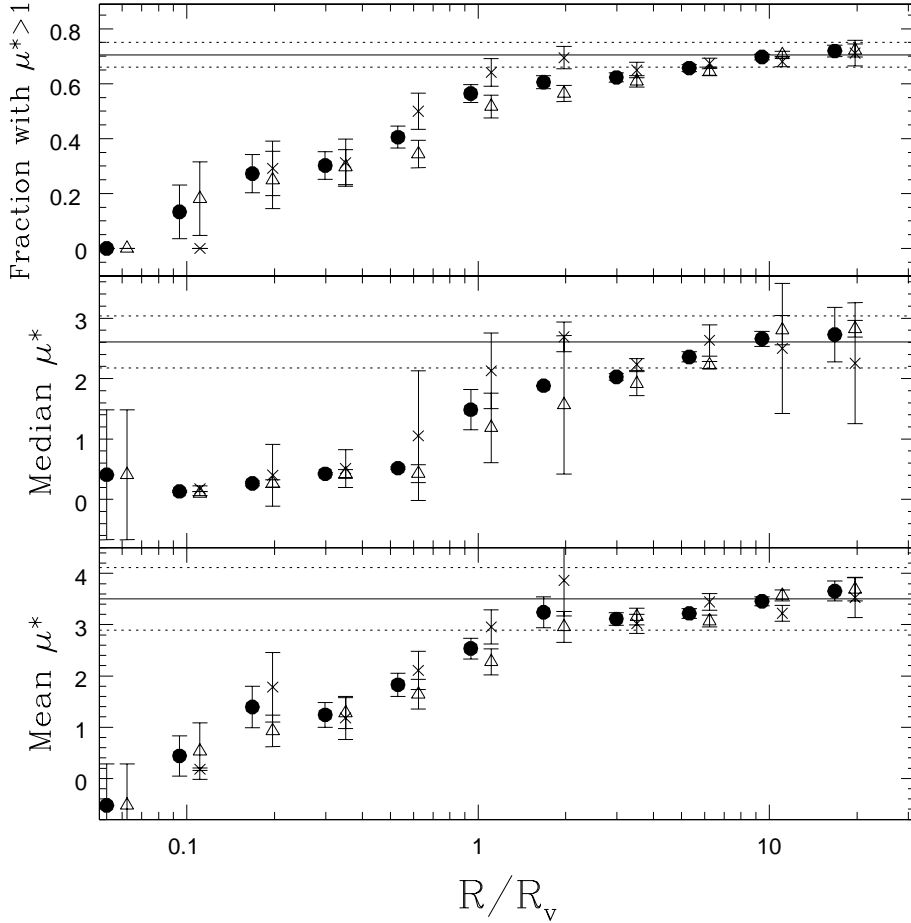


Fig. 1.7. Star formation rate as a function of cluster-centric radius, derived from our 2dFGRS analysis. *Filled* points represent the full galaxy sample, while the *triangles* and *crosses* represent the “high”- and “low”-velocity dispersion clusters (see text for details). The *solid horizontal* lines represent the value of each statistic for our field galaxy sample.

equivalent width rather than line flux measurements are possible with the 2dFGRS spectra, we can only infer the SFR,  $\mu$ , per unit luminosity:  $\mu/L_{\text{cont}} = 7.9 \times 10^{-42} \text{ EW(H}\alpha\text{)}$ , using Kennicutt’s (1992) SFR-EW(H $\alpha$ ) relation. We then normalized this to a characteristic luminosity  $L^*$ :  $\mu^* = \mu/(L_{\text{cont}}/L^*) = 0.087 \text{ EW(H}\alpha\text{)}$ , where  $L^*$  is taken to be the knee in the luminosity function in the  $r'$  band (near rest-frame H $\alpha$ ), as determined by Blanton et al. (2001).

In Figure 1.7, the mean and median value of  $\mu^*$  is plotted as a function of the projected cluster-centric radius. Here the latter has been normalized by the cluster virial radius,  $R_v$ , which has been calculated for each individual cluster and ranges from 1.4 to 2.4 Mpc. Also plotted in the top panel of Figure 1.7 is the fraction of galaxies with  $\mu^* > 1 M_\odot \text{ yr}^{-1}$ , which

represents the tail of the distribution, comprised of galaxies that are currently forming stars at a high rate relative to their luminosities. The solid horizontal line represents the values derived for the “field” galaxies within our sample, that is, galaxies that lie within the 20 Mpc selection radius, but which, from their redshifts, are identified as non-members. The bracketing dashed horizontal lines represent the  $1\sigma$  standard deviation from field to field, giving some estimate of the cosmological variance in the field value.

Irrespective of which statistic is used, it is very clear that within the clusters  $\mu^*$  falls significantly below the value of the field, the difference being at a maximum at the cluster center and then monotonically decreasing with increasing cluster-centric radius. *Importantly, convergence does not occur until  $R > 3R_v$ !* Hence, compared to the field, cluster galaxies differ in their mean star formation properties as far out as  $\sim 6$  Mpc from their centers. Also of note is that these radial trends in  $\mu^*$  appear to be insensitive to cluster mass, with there being no discernible difference between the “high”- and “low”-velocity dispersion clusters.

Such a radial analysis, however, is likely to be sub-optimal, since many of the clusters in our sample are clearly not spherically symmetric and show substructure. We have therefore analyzed  $\mu^*$  as a function of the local projected galaxy density,  $\Sigma$ , based on the distance to the tenth nearest neighbor (Dressler 1980). The relationship between  $\mu^*$  and  $\Sigma$  is shown in Figure 1.8, using the same three statistics that we used in the radial analysis. The vertical line shows the mean value of  $\Sigma$  within  $R_v$ , and once again the horizontal lines show  $\mu^*$  and its  $1\sigma$  variance for the field.

We see that cluster galaxy star formation is suppressed relative to the field, the difference being greatest at the highest local densities, and decreasing monotonically with decreasing density until the two converge at  $\Sigma \approx 1.5$  galaxy Mpc $^{-2}$ , a factor of  $\sim 2.5$  times lower than the mean projected density of the cluster virialized region. Yet again the trend is no different in the “high”- and “low”-velocity dispersion clusters, indicating that SFRs depend only on the local density, regardless of the large-scale structure in which they are embedded. Further evidence that local density is the key variant is also provided by a plot based on just those galaxies with  $R > 2R_v$ , where the same trend observed for the full sample is seen. This would suggest that a more general view of star formation suppression be taken: that it will be low relative to the global average in *any* region where the local density exceeds a value of  $\sim 1$  gal Mpc $^{-2}$  ( $M_b \leq -19$  mag).

It is well known that galaxy morphology is very strongly correlated with local galaxy density (Dressler 1980), and hence consideration needs to be given to what underlying contribution this has to the  $\mu^* - \Sigma$  relationship seen in Figure 1.8. Using a simple model based on Dressler’s morphology-density relation, we have calculated the expected variation in  $\mu^*$ ; this is represented by the *solid curves* in Figure 1.8. This appears to be shallower than the observed relation, suggesting that the morphology-density relation is distinct from the SFR-density relation, with additional processes operating at  $\Sigma > 1$  galaxy Mpc $^{-2}$  that drive  $\mu^*$  significantly below that expected on the basis of the changing morphological mix. Indeed, it may well be the case that the suppression of star formation is the primary transformation that occurs with environment, with the change in morphological mix being a secondary effect (Poggianti et al. 1999; Shioya et al. 2002)

A complete description of this study and a full discussion of its implications can be found in Lewis et al. (2002).

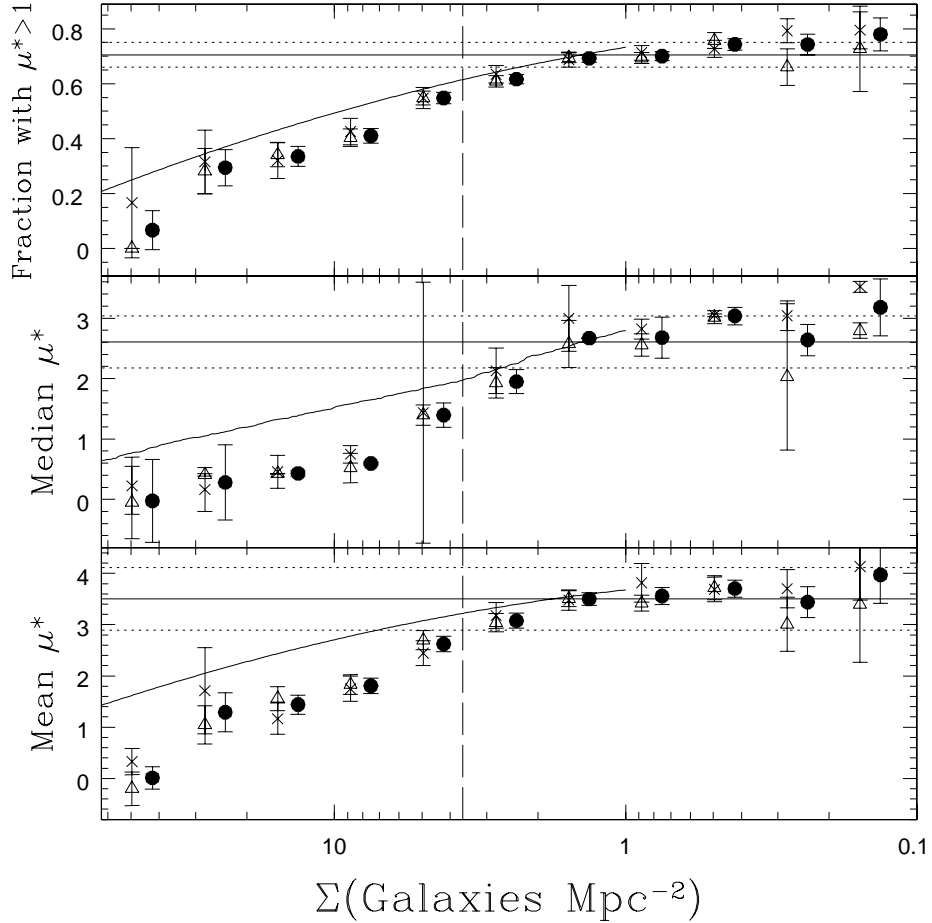


Fig. 1.8. Star formation rate as a function of local projected galaxy density,  $\Sigma$ . The *dashed* vertical line represents the mean value of  $\Sigma$  within  $R_v$ . The *curved* lines indicate the variation expected as a result of the varying morphological mix.

#### 1.4.2 Within Galaxy Groups

Extension of this analysis to the galaxy group environment has just recently become possible through the 2dFGRS being subjected to a 3D “friends-of-friends” analysis to identify groups (and clusters) in both position and redshift space (Eke et al. 2003). This has produced a catalog containing  $\sim 30,000$  groups with at least 2 members; their distribution within the two 2dFGRS strips is shown in Figure 1.9. The star formation properties of this sample are currently being analyzed, and we show here (courtesy of Dr. M. Balogh) a couple of very preliminary results that give the first indications of environmental trends in these much poorer, lower-velocity dispersion analogs to rich clusters.

Once again the  $H\alpha$  line has been used as a measure of SFR, with it being identified and its equivalent width measured in the spectra of all group members in identical fashion to

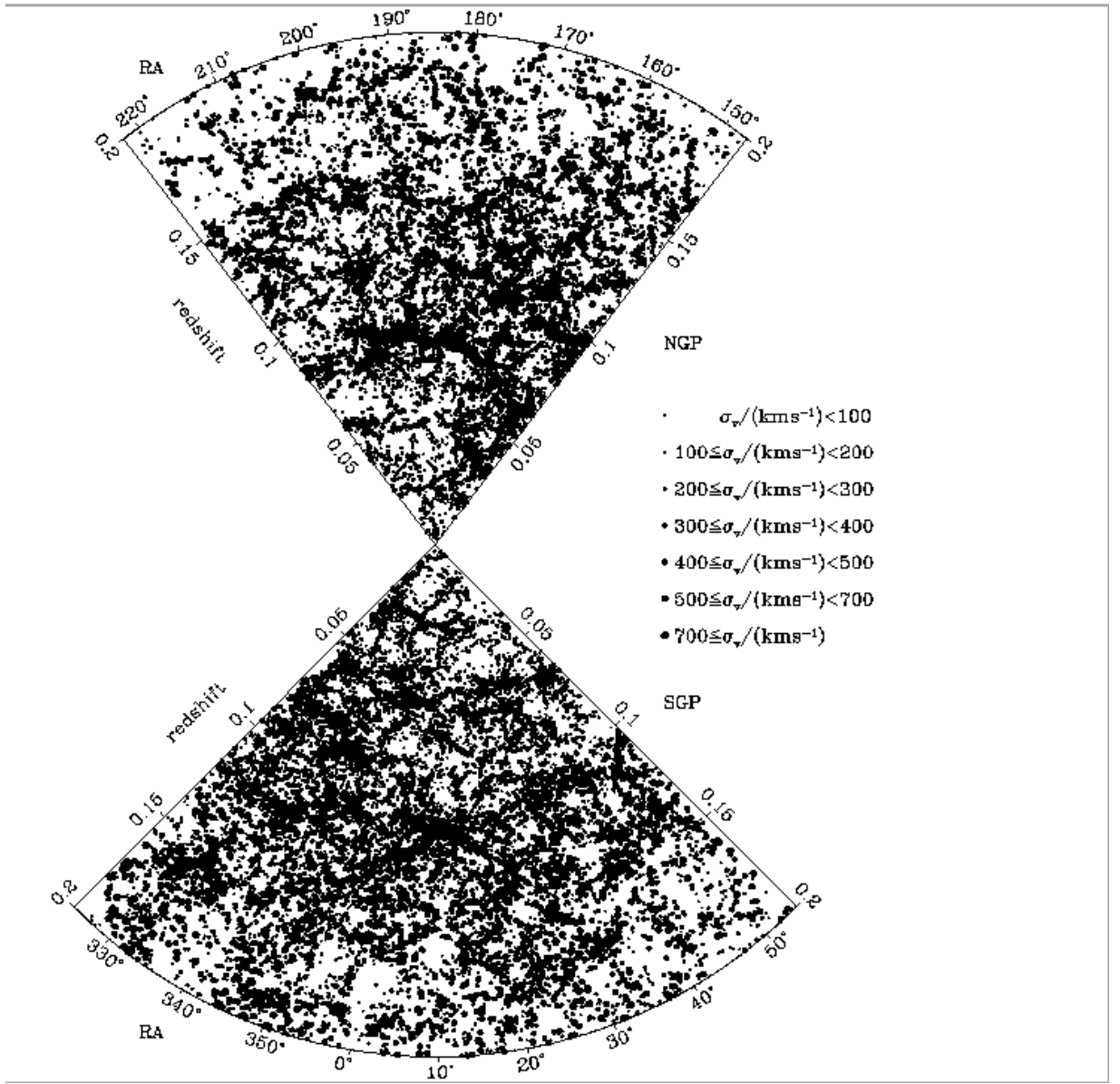


Fig. 1.9. A redshift slice showing the distribution of groups and clusters identified within the 2dFGRS using a 3D “friends-of-friends” analysis (Eke et al. 2003). The estimated velocity dispersion is shown by the size of the dot.

that described above for cluster galaxies. An overall  $\text{H}\alpha$  equivalent width was then derived for each group taking the mean value of all its members. In Figure 1.10 this mean value is plotted as a function of group velocity dispersion, being represented by all the individual dots. To assess whether there is any overall trend, the data have been divided into equally

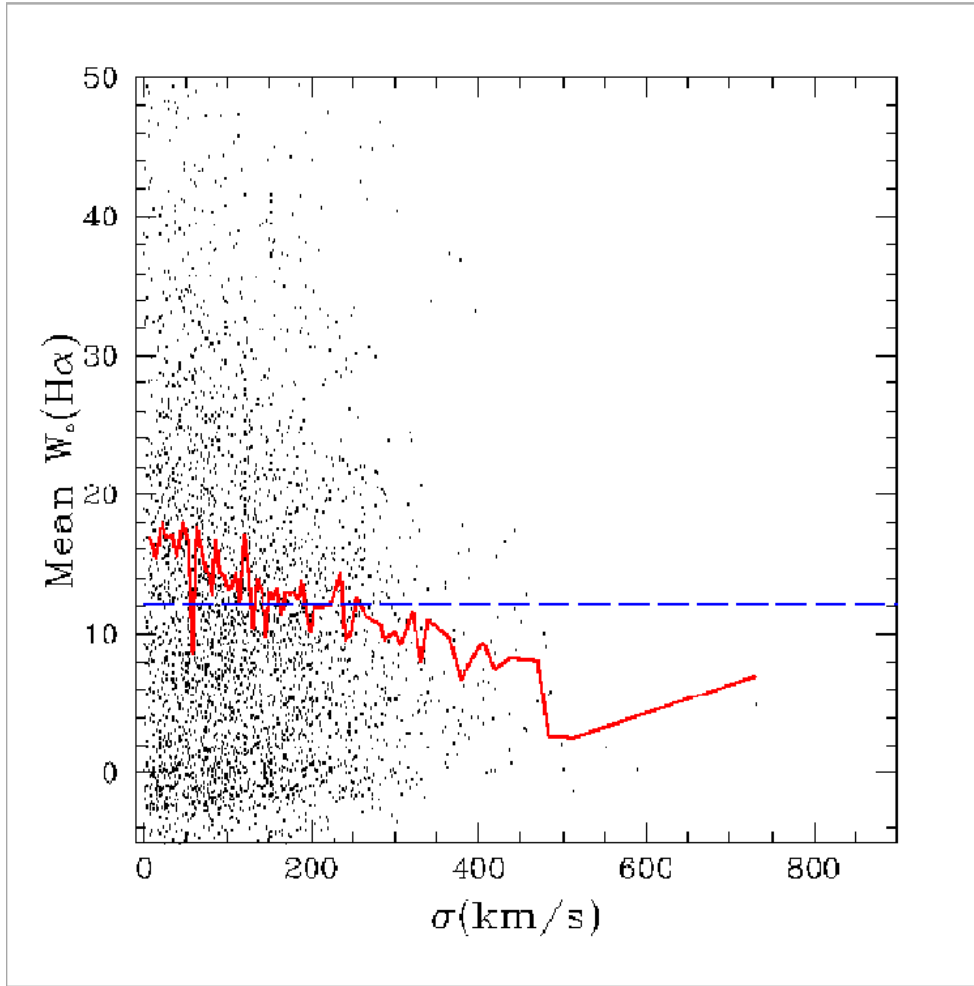


Fig. 1.10. The mean equivalent width of  $\text{H}\alpha$  for groups within the 2dFGRS versus their velocity dispersion. The *dots* represent individual groups whose values have been determined from their member galaxies; the *solid line* connects the mean values evaluated within equally populated velocity dispersion bins; the *dashed* horizontal line indicates the mean value for “field” galaxies.

populated velocity dispersion bins and averaged; the continuous line has been drawn through these average values. As a comparison, the mean  $\text{H}\alpha$  equivalent width for “field” galaxies — those galaxies identified as not belonging to any group within the friends-of-friends analysis — is shown as the horizontal dashed line.

It can be seen in Figure 1.10 that there is a noisy but significant trend of  $\text{H}\alpha$  emission (and hence SFR) becoming increasingly stronger with lower group velocity dispersion. Intriguingly, however, this trend intersects the horizontal “field” line at  $\sigma \approx 250 \text{ km s}^{-1}$ , indicating that there are not only groups whose mean  $\text{EW}(\text{H}\alpha)$  is below that of the field (as might be expected from the SFR– $\Sigma$  relation observed in the rich cluster study), but also groups whose

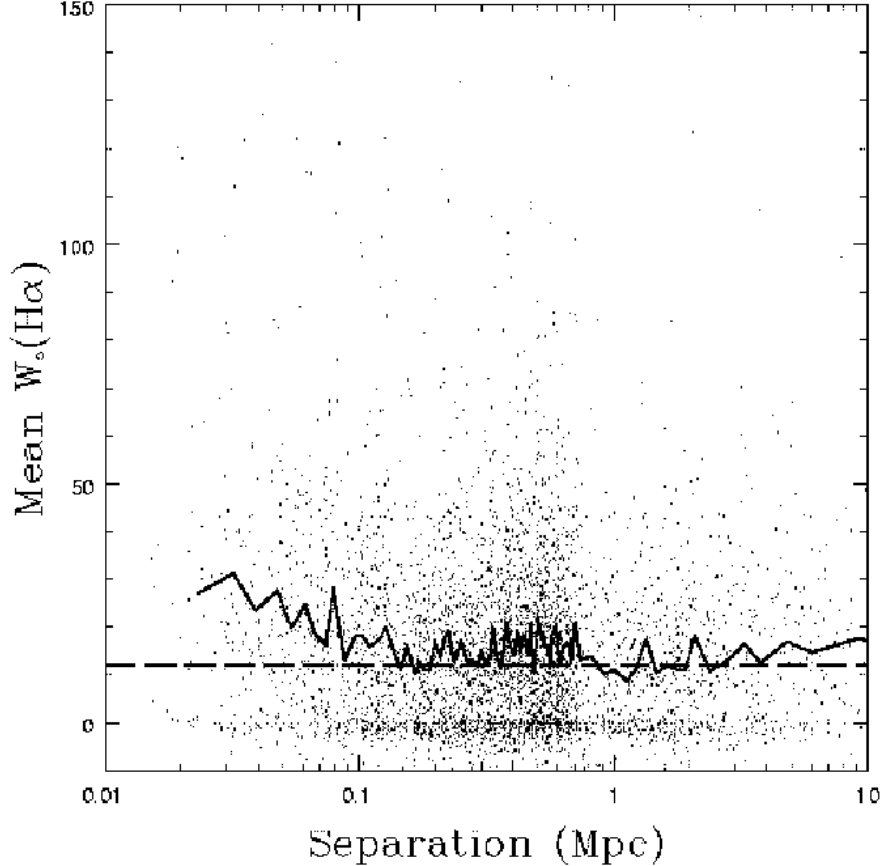


Fig. 1.11. The mean equivalent width of  $H\alpha$  for binary groups with velocity dispersions  $\sigma < 150 \text{ km s}^{-1}$ , plotted as a function of the separation between the two galaxies. The *dots* represent individual groups; the *solid line* connects the mean values evaluated within equally populated galaxy separation bins; the *dashed horizontal line* indicates the mean  $H\alpha$  equivalent width for field galaxies.

mean  $\text{EW}(H\alpha)$  is *higher* than the field, hinting that star formation activity is for some reason enhanced (cf. the field) in these lower-velocity dispersion ( $\sigma < 150 \text{ km s}^{-1}$ ) groups.

The underlying reason for this may well be contained in Figure 1.11, where we show the mean  $\text{EW}(H\alpha)$  for just the *binary* groups within the  $\sigma < 150 \text{ km s}^{-1}$  regime, plotted as a function of their separation (in Mpc). Yet again, the equal-numbered bin averaging and the benchmark “field” value are represented in the same way as in Figure 1.10. We see that for separations in the range  $0.1\text{--}10 h^{-1} \text{ Mpc}$ , binary groups have, to within the fluctuations, the same mean  $\text{EW}(H\alpha)$  as the field. However, at separations below  $0.1 h^{-1} \text{ Mpc}$ , the mean  $\text{EW}(H\alpha)$  for binary groups is seen to be significantly higher than the field. Although this is

*W. J. Couch, M. M. Colless, and R. De Propris*

yet to be fully investigated, it is suggestive that the enhanced SFRs seen in the low-velocity dispersion groups (relative to the field) can be attributed to “close” binary systems where tidal interactions may well be responsible for this activity.

**Acknowledgments.** These results are presented on behalf of the 2dFGRS team: Ivan Baldry, Carlton Baugh, Joss Bland-Hawthorn, Sarah Bridle, Terry Bridges, Russell Cannon, Shaun Cole, Matthew Colless, Chris Collins, Warrick Couch, Nicholas Cross, Gavin Dalton, Roberto De Propris, Simon Driver, George Efstathiou, Richard Ellis, Carlos Frenk, Karl Glazebrook, Edward Hawkins, Carole Jackson, Bryn Jones, Ofer Lahav, Ian Lewis, Stuart Lumsden, Steve Maddox, Darren Madgwick, Peder Norberg, John Peacock, Will Percival, Bruce Peterson, Wil Sutherland, and Keith Taylor. The 2dFGRS was made possible through the dedicated efforts of the staff of the Anglo-Australian Observatory, both in creating the 2dF instrument and in supporting it on the telescope. W.J.C. and R.D.P. acknowledge funding from the Australian Research Council throughout the course of this work.

## References

Abell, G. O. 1958, *ApJS*, 3, 211  
 Abell, G. O., Corwin, H. C., & Olowin, R. 1989, *ApJS*, 70, 1  
 Blanton, M. R., et al. 2001, *AJ*, 121, 2358  
 Butcher, H., & Oemler, A., Jr. 1978, *ApJ*, 219, 18  
 Colless, M. 2003, in *Carnegie Observatories Astrophysics Series*, Vol. 2: *Measuring and Modeling the Universe*, ed. W. L. Freedman (Cambridge: Cambridge Univ. Press)  
 Colless, M., et al. 2001, *MNRAS*, 328, 1039  
 Dalton, G. B., Maddox, S. J., Sutherland, W. J., & Efstathiou, G. 1997, *MNRAS*, 289, 263  
 De Propris, R., et al. 2002, *MNRAS*, 329, 87  
 —. 2003, *MNRAS*, 342, 725  
 Dressler, A. 1980, *ApJ*, 236, 351  
 —. 2003, in *Carnegie Observatories Astrophysics Series*, Vol. 3: *Clusters of Galaxies: Probes of Cosmological Structure and Galaxy Evolution*, ed. J. S. Mulchaey, A. Dressler, & A. Oemler (Cambridge: Cambridge Univ. Press)  
 Eke, V. R., et al. 2003, *MNRAS*, submitted  
 Elgarøy, O., et al. 2002, *Phys. Rev. Lett.*, 89, 061301  
 Folkes, S. R., et al. 1999, *MNRAS*, 308, 459  
 Kennicutt, R. C., Jr. 1992, *ApJS*, 79, 255  
 Lahav, O., et al. 2002, *MNRAS*, 333, 961  
 Lewis, I. J., et al. 2002, *MNRAS*, 334, 673  
 Lumsden, S. L., Nichol, R. C., Collins, C. A., & Guzzo, L. 1992, *MNRAS*, 258, 1  
 Madgwick, D. S., et al. 2002, *MNRAS*, 333, 133  
 —. 2003, *MNRAS*, submitted (astro-ph/0303668)  
 Nichol, R. C. 2003, in *Carnegie Observatories Astrophysics Series*, Vol. 3: *Clusters of Galaxies: Probes of Cosmological Structure and Galaxy Evolution*, ed. J. S. Mulchaey, A. Dressler, & A. Oemler (Cambridge: Cambridge Univ. Press)  
 Norberg, P., et al. 2001, *MNRAS*, 328, 64  
 Oemler, A., Jr. 1974, *ApJ*, 194, 1  
 Peacock, J. A., et al. 2001, *Nature*, 410, 169  
 Percival, W. J., et al. 2001, *MNRAS*, 327, 1297  
 Poggianti, B. M., Smail, I., Dressler, A., Couch, W. J., Barger, A. J., Butcher, H., Ellis, R. S., & Oemler, A. 1999, *ApJ*, 518, 576  
 Schechter, P. L. 1976, *ApJ*, 203, 279  
 Shioya, Y., Bekki, K., Couch, W. J., & De Propris, R. 2002, *ApJ*, 565, 223  
 Verde, L., et al. 2002, *MNRAS*, 335, 432